## PAPER

# Non-woven pitch-based carbon fiber electrodes for low-cost redox flow battery†

Abena A. Williams, ‡ Sagar V. Kanhere, ‡ Amod A. Ogale
and Mark E. Roberts *

Redox flow batteries (RFBs) are promising energy storage systems to support renewable energy sources and overcome the limitations imposed by their intermittent and unpredictable nature. As a developing technology, the cost of key components, namely the membrane, electrolyte, and electrodes, present a major hurdle to widespread integration. This work describes the performance of non-woven carbon fiber (NWCF) electrodes derived from low-cost petroleum pitch and produced using a scalable, inexpensive melt-blowing process. Compared to commercial polyacrylonitrile (PAN)-based carbon fiber felt, pitch-based carbon fibers have increased graphitic content, tensile strength, and electrical conductivity. Greenhouse gas emissions for pitch-based carbon fibers are estimated to be significantly lower than that of PAN-based carbon fibers. When RFBs with unoptimized NWCF electrodes are evaluated in zinc iodide electrolytes, the voltage and power density (83 mW cm$^{-2}$) are slightly lower compared to RFBs with PAN-derived carbon felts (104 mW cm$^{-2}$) @ 100 mA cm$^{-2}$. RFBs fabricated with oxidized low-cost NWCF electrodes show nearly identical battery performance to those prepared with commercial PAN-derived carbon felts in vanadium electrolytes (peak power density of 137 mW cm$^{-2}$ *vs.* 139 mW cm$^{-2}$, respectively). Because of their low-cost precursor and cheaper processing methods, NWCF electrodes offer a promising solution to reducing the cost of RFB electrode materials, and with further optimization, these electrodes will likely result in improved battery performance.

## Introduction

With increasing global energy demands and goals to reduce our dependence on carbon emitting fuels, electricity generation from renewable sources, such as wind and solar, has seen tremendous growth over the past two decades.[1,2] Because of the intermittent nature of these sources, it is necessary to develop low-cost Long Duration Energy Storage (LDES) systems to support their integration into the electric grid and maintain stability or deploy them as stand-alone electricity generation sources.[3,4] The current solution to address the variable energy supply is the use of natural gas powered generators;[5,6] however, this backup system, while extremely reliable, is very expensive and contributes to greenhouse gas emissions.[7,8] Other emission-free options, such as Pumped-Storage Hydropower stations, cause significant environmental damage and are not feasible at different scales. Energy storage systems must be efficient, safe, and cost-effective for sustainable energy transition to be considered options for long-duration energy storage of renewable sources. Current commercial options for LDES include Pumped-Storage Hydropower (PSH) and Compressed Air Energy Storage (CAES), both of which depend on geographical forms, and are hard to deploy on grid-scale applications.[9]

Redox flow batteries (RFBs) are an emerging energy storage technology that is unique from other types of batteries because the power and energy outputs are decoupled.[10–13] Charge is stored in electrolytes comprising active ion species (contained in external tanks), which are pumped through porous carbon electrodes where charging/discharging occurs.[14,15] The energy is dependent upon the size of the tanks and the concentration of the ions, while the power is governed by the size of the electrode stack and the properties of the electrode.[11,16,17] The state-of-the-art RFB uses vanadium in the electrolyte, a Nafion™ membrane, and PAN-derived carbon felt electrodes.[18–20] The cost estimate of this type of RFB is about $252 per kW h, with about 40% attributed to the Nafion, 30% to the vanadium, and about 12% to the electrodes (or $32 per kW h).[21] The cost of each of these components must be reduced to reach the Department of Energy (DOE) price target of <$100 per kW h to achieve market acceptance.[22,23] Most research on reducing the cost of RFBs focuses on developing alternative, lower-cost membranes[24] or new electrolytes based on abundant redox materials, such as iron[25–28] or zinc,[29–32] with limited attention given to the electrode material. Electrode materials also

*Center for Advanced Engineering Fibers and Films, Department of Chemical Engineering, Clemson University, Clemson, SC 29634, USA. E-mail: mrober9@clemson.edu*

† Electronic supplementary information (ESI) available. See DOI: https://doi.org/10.1039/d4se01124d

‡ Authors contributed equally.

contribute significantly to GHG emissions among all components of RFBs, second to electrolytes.[33]

Electrode materials for RFBs must be electrochemically and mechanically stable, conductive, and wettable by the electrolyte to facilitate the charge-transfer reactions at the solid–liquid interface. Carbon in the form of nanofibers in a felt or cloth is being investigated because it's inert, relatively low-cost and conductive compared to other alternatives; however, they are expensive to produce and can lead to high pressure drop across the felt.[19,34] Commercial PAN-based carbon electrodes are prepared by conventional textile nonwoven methods such as needle punching; however, the fibers are made using either roll spinning or electrospinning, both of which require solvents and a coagulation bath.[35] The electrospinning method, however, is difficult to scale up and requires additives to the polymer solution.[36] About half of the cost of carbon filament comes from the cost of the precursor itself, and since PAN is an expensive precursor, lower-cost alternatives have been investigated. Rayon-based carbon felts have received attention, but they are limited by low carbon yield (25% compared to 40% for PAN),[37] relatively low conductivity, and higher overall fiber cost ($36 per lb compared to $15 per lb for PAN).[35] Furthermore, Rayon-based carbon fibers are more susceptible to oxidation than PAN-based carbon at high state of charge.[38] Lignin-based carbon electrodes are proposed as an alternative, but they are just in the research phase and are yet to be commercialized.[39] Because carbon fiber electrodes are generally hydrophobic, electrodes are often oxidized or pretreated to improve their wettability and electrochemical activity.[40,41]

Carbon fibers can also be made from mesophase pitch, which is a low-cost precursor that is leftover as a byproduct from petroleum refining and is widely available and underutilized. With costs projected to be less than $2 per lb and carbon yields as high as 80%, pitch-based carbon fibers are an excellent alternative for PAN-based carbon electrodes.[42,43] They are also shown to have a lower environmental impact than their PAN-based carbon fiber alternatives.[44] Additionally, their highly oriented graphitic microstructure gives rise to excellent thermal and electrical conductivity.[43,45–47] As compared with PAN-derived carbon fibers, mesophase pitch-based carbon fibers possess three times higher electrical conductivity and double the modulus.[48,49] As a result, pitch-based carbon fibers are generally used for high stiffness reinforcement carbon fibers or thermal management and only some work has been reported as electrode material for Li-ion batteries.[50,51] Unlike PAN or rayon, pitch-based precursor fibers can be produced using melt-blowing, a low-cost and scalable process that can produce non-woven carbon fiber mats.[52,53] This is possible because mesophase pitch-based fibers form their microstructural orientation during fiber spinning step, and it is retained during stabilization and carbonization step.[46] From a sustainability standpoint, pitch-based carbon fibers have an estimated 68% reduction in greenhouse gas emissions compared to PAN-based carbon fibers due to less processing required to produce the precursor pitch.[54]

In this work, we present an alternative, low-cost non-woven carbon fiber (NWCF) electrode derived from petroleum pitch and produced using a scalable and inexpensive melt-blowing process. Compared to commercial PAN-derived carbon fiber felt, pitch-based NWCFs have increased graphitic content, tensile strength, and electrical conductivity at a fraction of the cost. RFBs fabricated with oxidized NWCF electrodes show nearly identical battery performance to those prepared with commercial PAN felts in vanadium electrolytes. When RFBs with NWCF electrodes are evaluated in a zinc iodide electrolyte, the voltage and power density are slightly lower compared to RFBs with PAN felts; however, the surface treatment of these materials is not yet optimized. Because the precursor and processing methods are both inexpensive relative to PAN-based fibers, NWCF electrodes offer a promising solution to minimizing the cost of RFB electrode material. Furthermore, with the optimization of carbon fiber synthesis and surface treatment, it is possible that these materials lead to improved battery performance.

## Experimental

### Non-woven pitch-based carbon felt

**Processing.** Non-woven pitch-based fiber mats were produced using the melt-blowing method. The pitch precursor, containing about 75% mesophase content, was extruded using 1-inch diameter single-screw extruder operating continuously through a proprietary design of spinnerets. The exiting fibers were pulled through an air aspirator (10–15 psig) that was held about 2–3 in below the spinnerets and collected on a mesh substrate connected to the vacuum. The fibers we stabilized in a forced air convection oven (Memmert GmbH + Co, Schwabach, Germany) and carbonized at 2100 °C in an Astro 1000 furnace (Thermal Technology, LLC).

**Carbon fiber properties.** Electrical resistance ($R$) of single fibers was measured by first mounting single filaments on paper tabs that were then placed between two copper wires separated by 10 mm. Using this known length and area (calculated from measured diameters of the fiber), electrical resistivity was calculated. Tensile analysis of carbon fibers was based on the ASTM D3379-75 standard test procedure.[55] A single fiber was mounted on a paper tab with a 10 mm gauge length and bonded to the tab using epoxy resin. After curing of epoxy resin, the sides of the tab were burned away within the grips of a MTI Phoenix testing machine, fiber was then stressed to failure at a constant strain rate of 0.5 mm min$^{-1}$. Cross-sectional area of the fiber was determined by measuring the diameter of individual filaments using Olympus BX60 optical microscope. Preliminary elemental analysis of the carbon fiber surface was performed by Energy DispersiveSpectroscopy using Oxford Instrument Detector at 20 kV beam voltage and 10 μA beam current.

**Microstructural characterization.** To analyze the cross-sectional microstructure and longitudinal surface of the carbon fibers, scanning electron microscopy was conducted on samples using high-resolution FESEM scopes (S4800/SU5000, Hitachi). For Raman analysis, individual filaments were scanned under Renishaw inVia Raman microscope with laser wavelength of 785 nm and laser power of 25 mW. The incident

beam was focused on fiber surface using 50× objective lens. The collected spectra were analyzed using WiRE Raman Software version 3.4. A silicon standard with Raman shift at 520 cm$^{-1}$ was used to calibrate the detector. Wide-Angle X-ray Diffraction analysis was conducted using a Rigaku SmartLab Powder Diffractometer with Cu Kα radiation source (0.15406 nm) and Hypix3000 detector. The location of the $2\theta$ peaks was calibrated using NIST Silicon standard.

### Electrochemical characteristics

**Electrochemical characterization of redox electrolytes.** Cyclic voltammetry experiments were conducted in a three-electrode cell using VersaStat 4 (VersaStudio, Princeton Applied Research). Ag/AgCl was used as the reference electrode, a graphite rod was used as the counter electrode, and a glassy carbon electrode (GCE) from BASi (BASi MF 2012) was used as the working electrode. The vanadium electrolyte was 1.0 M vanadium(IV) sulfate oxide hydrate (BeanTown Chemicals) in 3.0 M sulfuric acid (Fisher Scientific). Vanadium(IV) was converted to vanadium(III) by charging at 1.8 V until the current decreased below 10 mA. The zinc iodine electrolyte contained 1.0 M potassium iodide (Acros Organics) and 0.5 M zinc bromide (ThermoFisher Scientific) in a 1.0 M potassium chloride (Sigma-Aldrich) solution.

**Redox flow battery assembly and electrochemical testing.** Lab-scale redox flow batteries from ElectroCell were assembled with a 10 cm$^2$ electrode area. All electrical tests were conducted on an Arbin Instruments (MSTAT21044) battery analyzer, and a multi-head peristaltic pump from Chonry was used to circulate electrolytes through the cells. The electrode materials were either non-woven carbon fiber (NWCF) mats or PAN-based carbon felts (Ceramaterials, GFE-1 specialty felt) that were previously soaked in redox electrolyte overnight. For comparison to pretreated PAN felts, NWCF electrodes were oxidized using potassium permanganate (Fisher Scientific) at 80 °C.[56,57]

For the V RFB, a Nafion 117 (178 μm) membrane was used with 50 mL of electrolyte in each tank. The membrane was activated by refluxing at 90 °C for 1 h each with DI water, 3 v% hydrogen peroxide (30% Fisher), DI water, 0.5 M sulfuric acid (98% Fisher), DI water, and 3 M sulfuric acid. The membrane was stored in 3 M sulfuric acid until use. VOSO$_4$ (V$^{4+}$) was used as both catholyte and anolyte. The battery was charged at 50 mA cm$^{-2}$ until 1.8 V, then charged at 1.8 V until the current decreased below 10 mA (the catholyte was converted to V$^{5+}$ and the anolyte was converted to V$^{3+}$). The catholyte (V$^{5+}$) was replaced with the original VOSO$_4$ (V$^{4+}$) solution and the battery was charged again to convert the catholyte to V$^{5+}$ and the anolyte to V$^{2+}$. N$_2$ gas was bubbled through both tanks to prevent the oxidation of vanadium ions. Polarization curves were developed on the fully charged battery (current less than 10 mA at 1.8 V) by discharging the battery for 30 s time periods from low to high current densities with a 30 s rest period between each current density. Charge discharge tests were done at varying current densities by charging to 1.8 V for low current densities (15 and 20 mA cm$^{-2}$) and 1.85 V for high current densities (30, 35, and 40 mA cm$^{-2}$), then discharging to 0.8 V.

Cycling tests were performed by first charging the battery partially at a current density of 10 mA cm$^{-2}$ to a voltage of 1.8 V, and the repeated charge discharge at a current density of 20 mA cm$^{-2}$ with limits of 1.8 and 0.8 V for charge and discharge, respectively.

For the ZI RFB, Nafion 212 (50 μm) was used as the membrane, and 125 mL of electrolyte was used in each tank. The membrane was activated by refluxing at 90 °C for 1 h each with DI water, 3 v% hydrogen peroxide, DI water, 0.5 M sulfuric acid, DI water, and 1 M potassium chloride (Alfa Aesar). The activated membrane was stored in 1 M potassium chloride until use. Battery conditioning was performed by charging for 0.1Ah and then discharging to 0.8 V at current densities of 10, 20 and 40 mA cm$^{-2}$. Polarization curves were developed as described above on a fully charged battery (by applying 10 mA cm$^{-2}$ to 1.5 V). For charge–discharge tests, upper voltage limits were 1.65 V for current densities of 35 and 30 mA cm$^{-2}$, 1.6 V for 25 and 20 mA cm$^{-2}$ and 1.5 V for 10 mA cm$^{-2}$. The discharge limit for all current densities was 0.8 V. Long-term cycling was performed at 25 mA cm$^{-2}$ with limits of charge discharge voltage 1.55 V and 0.8 V.

## Results and discussion

### Characteristics of non-woven CFs

Carbon fiber electrodes were produced from mesophase pitch (∼75% mesophase content) using a melt-blowing process to create low-cost electrode materials for redox flow batteries. Fibers were drawn to a target diameter using the melt-blowing apparatus shown in the schematic in Fig. 1(a). Mesophase pitch fiber mats were collected on a mesh that was connected to vacuum suction. These fibers were then stabilized at 220 °C and carbonized at 2100 °C, resulting in a carbon fiber non-woven felt, as shown in Fig. 1(b). Because the fibers can be continuously blown into non-woven mat, this process is highly scalable, and NWCF felts as large as 6-inch × 4-inch have been produced. Furthermore, no additional solvents or coagulation baths are required, and the fibers do not need to be stretched to obtain highly graphitic content (discussed below).

The tensile and electrical properties of carbon fibers prepared from mesophase pitch were evaluated and compared with fibers from commercial PAN-based felts. Scanning electron microscopy (SEM) images of fiber surfaces and cross-sections
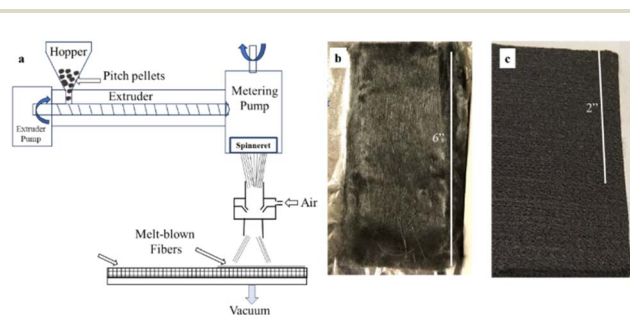


**Fig. 1** (a) Schematics of melt-blowing processing equipment (b) NWCF (c) PAN-derived felt.
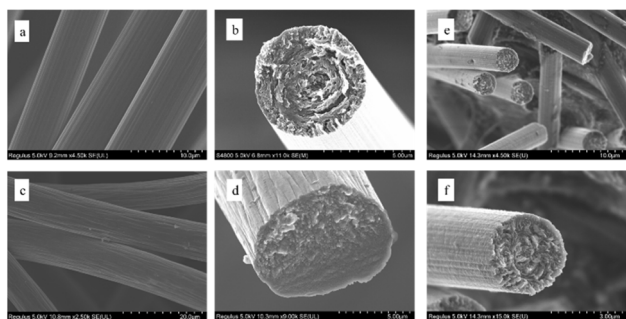
**Fig. 2** SEM micrographs of (a and b) non-woven pitch-based carbon fibers, (c and d) commercial PAN-derived carbon felt, (e and f) KMnO₄ treated non-woven pitch-based carbon fibers.

are shown in Fig. 2 for mesophase pitch-based fibers (a and b) and PAN-based fibers (c and d), respectively. The diameter of carbon fibers from the NWCF electrodes is $7.1 \pm 0.7 \mu m$, whereas that of PAN-based fibers is $10 \pm 1 \mu m$. As evident from the SEM images, PAN-based carbon fibers (from within the felt) show granular carbon structure, whereas pitch-based fibers (from within the NWCF mat) show highly ordered graphitic development with graphitic edges directed towards the lateral surface. The graphitic edge plane orientation observed in the NWCFs is desired because sites on edge planes are generally considered to be more electrochemically active.[58]

The graphitic structure of carbon within the fibers from each electrode type was determined using Raman spectroscopy, which can measure the relative amount of $SP^2$ (graphitic like) vs. $SP^3$ (diamond like) carbon in a given material. Fig. 3(a) shows the resultant Raman spectra of PAN-derived carbon felt and NWCF electrodes. As evidenced by the more pronounced G and D peaks, along with the presence of G′ and D′ peaks, carbon within the NWCF electrodes exhibit a more ordered, graphitic structure compared to carbon from the PAN-derived carbon felt. The $I_G/I_D$ ratio, which is the ratio of the area under the G and D peaks, respectively, is a quantitative indicator graphitic content. The carbon within the NWCF fibers had a substantially higher $I_G/I_D$ ratio of $0.6 \pm 0.1$ compared to that from PAN-derived carbon, $0.3 \pm 0.1$, which confirms the increased graphitic content observed in the SEM images.

Wide angle X-ray diffraction (WAXRD) was also used to evaluate the graphitic structure within the bulk material. As shown in Fig. 3(b), NWCF electrodes exhibited a sharp two-theta peak centered at 25.9°, whereas for PAN-derived carbon felt

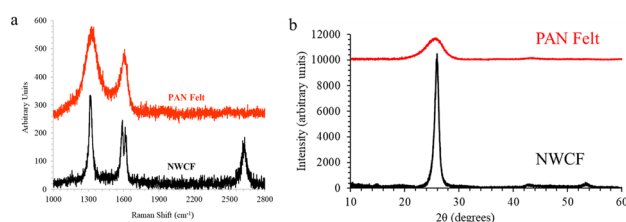showed a broad peak around 25.4°. The interlayer spacing (d002) is calculated using Bragg's law, yielding a value of 0.35 nm for PAN-derived carbon felt fibers and 0.34 nm for NWCF fibers. Using the Scherrer equation, it is estimated that the NWCF electrodes have a layer stacking height ($L_c$) of 4 nm, which is double that of the PAN-derived felt fibers (2 nm). Thus, WAXRD analysis further confirms that NWCF electrodes possess a notably higher organized graphitic structure than PAN-derived carbon felt fibers, consistent with Raman analysis and also confirmed by TEM analysis (Fig. S4†).

Carbon fiber electrodes for redox flow batteries need to be durable to maintain structural integrity under cell compression and flow conditions and conductive to deliver current flow to and from the electrolyte. The tensile strength of carbon fibers within the commercial PAN-derived carbon felt were found to be $0.6 \pm 0.3$ GPa with a corresponding tensile modulus of 100 GPa. In contrast, the untreated NWCF carbon fibers had a notably higher tensile strength of $2.2 \pm 0.7$ GPa, but this decreased slightly to $1.5 \pm 0.7$ GPa after surface oxidation, while the tensile modulus remained around 250 GPa. Because of the improved mechanical properties, there is no concern for physical or mechanical degradation of the NWCF electrodes within a flow cell. Next, electrical resistivity of individual filaments of fibers from PAN-derived carbon felts and NWCF mats were measured using a 2 pt probe method. Carbon fibers from the PAN-derived carbon felt had a baseline electrical resistivity of $15 \pm 3 \mu\Omega$ m. Fibers from the NWCF mat, on the other hand, had a significantly lower electrical resistivity of $8 \pm 1 \mu\Omega$ m, which was expected because of their increased order and graphitic content relative to PAN-derived carbon felt. Thus, NWCF fibers exhibit improved mechanical and electrical properties compared to PAN-derived carbon felts, making them viable candidates for flow battery electrodes.

**Electrochemical testing**

Electrodes comprising NWCFs were evaluated in redox flow batteries using both vanadium(v) and zinc iodine (ZI) electrolytes and compared with RFBs assembled with PAN-derived carbon felt electrodes. Prior to battery testing, the redox behavior of the electrolytes was validated using a three-electrode cell with a standard glassy carbon (GC) working electrode, an Ag/AgCl reference and graphite rod counter electrode. Fig. 4(a) shows the cyclic voltammetry profiles at various scan rates in the vanadium electrolyte, with the anolyte in the negative potential range and the catholyte in the positive. As the voltage is decreased from 0 V vs. Ag/AgCl in the anolyte, $V^{3+}$ is reduced to $V^{2+}$ below −0.5 V, and then $V^{2+}$ oxidized back to $V^{3+}$ when the potential is increased back to 0. On the catholyte side, $V^{4+}$ is oxidized to $V^{5+}$ as the potential is increased above 0.9 V and then $V^{5+}$ converts back to $V^{4+}$ when the potential is reduced back to 0. Both sets of curves show excellent reversibility and stability, along with the expected linear increase in peak current with increasing scan rate, which is comparable to CV profiles performed on other carbon materials.[40,59]

The redox behavior of the zinc iodine electrolyte is shown in Fig. 4(b) on the same GC electrode at a scan rate of 10 mV s⁻¹.



**Fig. 3** (a) Raman spectra and (b) X-ray diffractogram of PAN-derived carbon felt and NWCF electrodes.
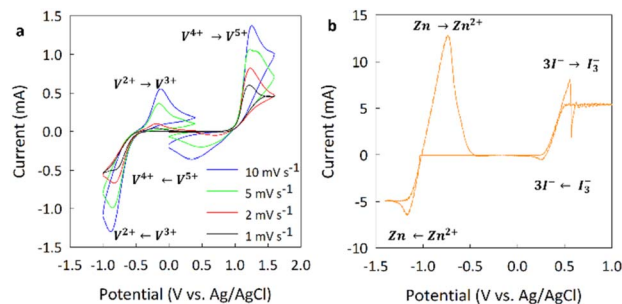
Fig. 4 Electrochemical characterization of redox electrolytes on glassy carbon electrodes. Cyclic voltammograms of (a) vanadium electrolyte at varying scan rates and (b) zinc iodine electrolyte at a scan rate of 10 mV s$^{-1}$.

Because the ZI system is symmetric, the same electrolyte is used for the catholyte and the anolyte, the cell was scanned over the combined potential range. The reversible oxidation of $3I^-$ to $I_3^-$ occurs the potential is increased above 0.4 V vs. Ag/AgCl and $Zn^{2+}$ is reduced Zn metal as the potential is decreased below $-1.0$ V, similar to previously reported results for ZI electrolytes on GC electrodes.[60] The $Zn/Zn^{2+}$ redox couple on the anolyte side exhibits low reversibility because of the zinc plating/stripping reactions occurring on the electrode, as evidenced by the asymmetric redox couple. Furthermore, it is difficult to obtain reproducible CV profiles at scan rates below 10 mV s$^{-1}$ without significantly reducing the concentration.

The performance of as synthesized NWCF electrodes in redox flow batteries was initially evaluated in lab-scale test cells

(see online ESI Fig. S1†) prior to any surface oxidation or treatment. RFBs assembled with vanadium redox chemistry were equipped with a Nafion 117 membrane and 50 mL electrolyte tanks. Fig. 5(a) shows the charge–discharge characteristics of RFBs with untreated NWCF electrodes with electrolyte circulating at a rate of 60 mL min$^{-1}$. The ordinate axis is normalized to volumetric capacity (Ah L$^{-1}$) by multiplying discharge time by current and dividing by tank volume. Because the electrolyte tank capacity is constant, the discharge curves would intercept this axis at the same value in the absence of any voltage losses or diffusion limitations. However, a large overpotential is observed at current densities as low as 15 mA cm$^{-2}$ resulting in a relatively low discharge voltage. The decrease in voltage is severe even at only moderately higher potentials, presumably due to the unoptimized electrode surface chemistry.

Polarization curves were developed on fully charged RFBs by measuring the discharge voltage with increasing current density until the discharge voltage reached 0. At each current density, beginning with 0.5 mA cm$^{-2}$, the batteries were discharged for 30 s followed by a 30 s rest period between applied currents. The discharge voltage is reported as the average voltage over the discharge period. Power density, obtained from Ohm's law ($P = I \times V$), is the product of the discharge current density and voltage. Fig. 5(b) shows the polarization curves for RFBs with untreated NWCF electrodes with electrolytes circulating at rates of 30 and 60 mL min$^{-1}$. As expected, higher flow rates resulted in higher discharge voltages because more active redox active species is available in a single pass through the electrodes.[61]
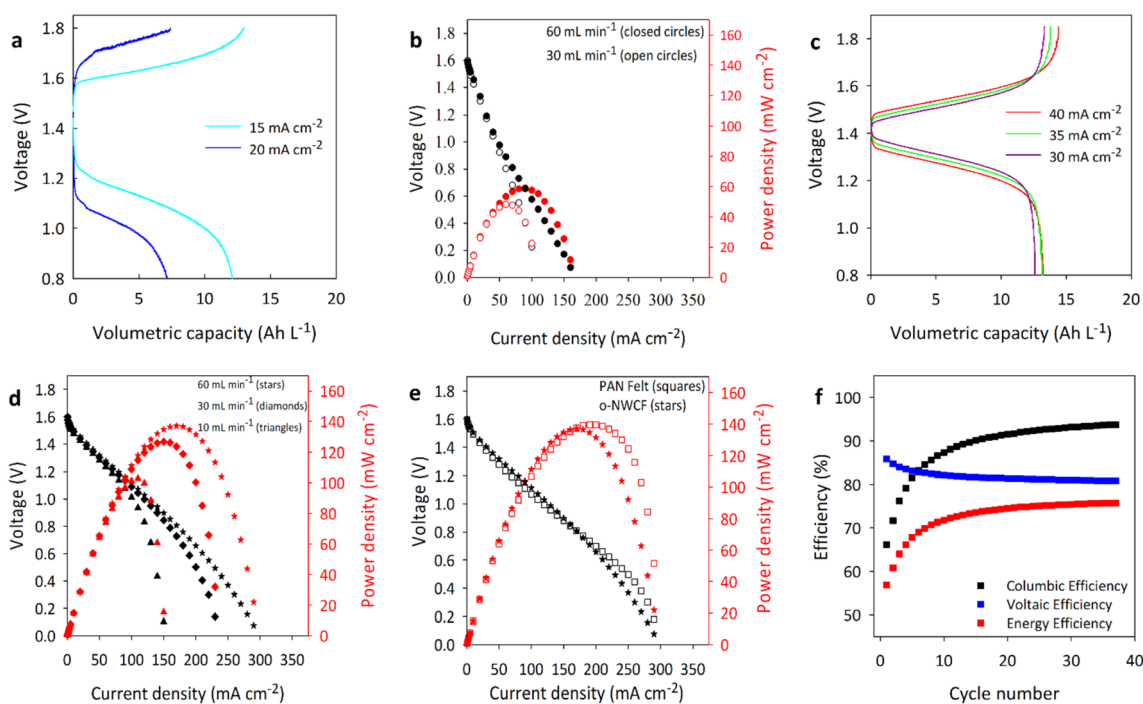


Fig. 5 Electrochemical performance of vanadium RFBs with NWCF electrodes. (a) Charge–discharge profiles and (b) polarization curves with untreated electrodes. (c) Charge–discharge profiles with KMnO$_4$-treated electrodes at 60 mL min$^{-1}$. (d) Polarization curves w with KMnO$_4$-treated electrodes at varying flowrates. (e) Comparison of KMnO$_4$-treated NWCF polarization curves to PAN-derived carbon felt at 60 mL min$^{-1}$. (f) Cycling efficiencies of KMnO$_4$-treated electrodes at 20 mA cm$^{-2}$ and 60 mL min$^{-1}$. Nafion 117 was used as the membrane in all VRFBs.

Regardless of the flow rate, discharge voltages were generally low, and the cells were unable to sustain high current densities. RFBs with untreated NWCF electrodes had a peak power density of 59 mW cm$^{-2}$ at 90 mA cm$^{-2}$, which is well below that obtained from RFBs with commercial PAN-derived carbon felt electrodes ($\sim$139 mW cm$^{-2}$ at 190 mA cm$^{-2}$).

While typical losses arise from the ohmic resistance of the membrane and electrode resistance,[62] here the performance is clearly limited by the electrode surface because all other components of the cell are identical. It's worth noting that the untreated NWCF electrodes are hard to wet, i.e. they did not readily absorb the electrolyte therefore, they had to be soaked overnight to become saturated with electrolytes prior to use in the RFB. Furthermore, RFBs with as-synthesized NWCF required extensive charge–discharge conditioning to achieve stable performance. Thus, untreated NWCF electrodes are likely insufficient for redox flow batteries using vanadium redox chemistry. However, commercial PAN-derived carbon felt electrodes have undergone extensive optimization of their surface treatment and activation to improve their interaction with the vanadium electrolyte.

The surface of carbon fiber based electrodes for vanadium redox flow batteries can be modified using various surface treatments, from chemical or thermal oxidation to vary surface chemistry, or activation to vary surface area and structure.[19,63,64] To provide a more relevant comparison to surface-activated PAN-derived carbon felt electrodes, the NWCF electrodes were oxidized using a previously reported chemical oxidation method with potassium permanganate.[56] Treatment of carbon fibers with KMnO$_4$ resulted in higher amounts of oxygen on the electrode surface, which is known to increase the rate of reaction due to increased wettability and number of reaction sites.[56,65,66] Accordingly, the oxygen content of NWCF electrodes increased from $(1.3 \pm 0.2)\%$ to $(4.3 \pm 0.8)\%$ after treatment with KMnO$_4$ without any observable difference in surface structure as shown in Fig. 2(e) and (f).

Fig. 5(c) shows the charge–discharge characteristics of KMnO$_4$-treated NWCF electrodes charged to 1.8 V and discharged to 0.8 V for current densities of 30–40 mA cm$^{-2}$. The ordinate axis is normalized to volumetric capacity as described above, which is approximately 13 Ah L$^{-1}$ regardless of the discharge current. Only slight decreases in discharge voltage were observed with increasing current density due to ohmic losses. Relative to RBFs with untreated NWCF electrodes, the voltage efficiency was significantly improved because of the decreased overpotential. This is attributed to the fact that chemical oxidation improves the wettability of the electrode, thus increasing electrolyte adhesion and utilization, and likely increases the number of reaction sites, and therefore reaction rate, at the electrode surface.[56] Improved electrolyte contact and higher charge transfer rates are evident by the decrease in overpotential even at moderately high current densities.

Polarization curves were developed on fully charged RFBs with KMnO$_4$-treated NWCF electrodes in a similar manner as those with untreated materials. Fig. 5(d) shows the polarization curves for these RFBs with electrolyte flow rates between 10 and 60 mL min$^{-1}$. The voltages reported are not IR-corrected

because the difference was not significant. As expected from improvements observed in charge–discharge behavior, RFBs with treated electrodes exhibited higher discharge voltages and could sustain higher currents than cells with untreated electrodes. Surprisingly, there was a negligible effect of flow rate on discharge voltage for current densities below 100 mA cm$^{-2}$ because the surface treatment eliminated reaction limitations under these conditions. An increase in discharge voltage is observed with increasing flow rates, which is typical for flow batteries, because the electrolyte channels are replenished with active redox species at rates necessary to support the current demand. The peak power density of 137 mW cm$^{-2}$ at 170 mA cm$^{-2}$ obtained represents a 132% increase compared to cells with untreated NWCF electrodes (59 mW cm$^{-2}$ at 90 mA cm$^{-2}$). This significant difference highlights the importance of surface properties on RFB performance, and the need to properly activate NWCF electrodes. Further optimization of the electrode surface treatment for vanadium chemistry is ongoing.

Redox flow batteries with PAN-derived carbon felt electrodes were prepared, controlling all other aspects of the cell, for comparison with the batteries comprising NWCF electrodes. Fig. 5(e) shows the polarization curves for cells with each electrode material using an electrolyte flow rate of 60 mL min$^{-1}$. While the discharge voltage and power density look similar for both batteries, some notable differences are present. First, the peak power density of the RFB with PAN-derived carbon felt (139 mW cm$^{-2}$) is slightly higher than those with NWCF (137 mW cm$^{-2}$). However, the higher performance with PAN-derived carbon felt is only realized for high current densities where the discharge voltage is prohibitively low for commercial operation (<0.8 V). In fact, for current densities up to $\sim$150 mA cm$^{-2}$, RFBs with NWCF electrodes outperform those with PAN-derived carbon felt. These results highlight the fact that a new class of carbon fiber electrodes derived from a low cost petroleum pitch precursor offers a suitable substitute to the conventional PAN-based electrode system to help drive down the cost of RFBs. As PAN-derived carbon felt electrodes have undergone substantial optimization to improve their performance in RFBs, we expect ongoing research on surface activation to further improve the performance of NWCF electrodes.

The stability of vanadium RFBs with NWCF electrodes was evaluated through continuous charge–discharge cycling at 20 mA cm$^{-2}$ and 60 mL min$^{-1}$ over 23 hours (or 37 cycles, charging to 1.8 V and discharging to 0.8 V). For each cycle, the coulombic, voltaic and energy efficiency were calculated and plotted, as shown in Fig. 5(f). The voltage efficiency slightly decreased over the first few cycles while the coulombic efficiency increased, which is in part due to the state of the battery before cycling (being charged at a higher current than cycling). After the initial break-in, or conditioning phase, the performance of the battery remained stable over 20 h or $\sim$35 cycles with no indication of impending degradation.

To reduce the cost of the RFB associated with the electrolyte, alternative redox chemistries have been studied as a replacement to vanadium. This includes iron[28,67] and zinc[31,68] based electrolytes mainly because of their low cost, high solubility, environmental friendliness, and natural abundance. As

opposed to vanadium-based electrolytes that are highly acidic, these systems are often based on alkali or neutral salts. Therefore, NWCF electrodes were also evaluated in a neutral zinc based electrolyte that varies in many ways from the vanadium system. RFBs were assembled using a symmetric zinc iodide electrolyte (same anolyte and catholyte) with Nafion 212 membranes, as described elsewhere.[29] In a similar manner as described above, RFBs with untreated NWCF electrodes were evaluated over a range of conditions and compared to batteries with KMnO₄-treated NWCF electrodes and commercial PAN-derived carbon felt electrodes.

Fig. 6 shows the performance of RFBs assembled with the various electrodes in the ZI electrolyte. Galvanostatic charge–discharge cycling of the RFB with untreated NWCF electrodes is shown in Fig. 6(a) with an electrolyte flow rate of 30 mL min⁻¹ for a range of current densities. For these cycles, the discharge voltage was limited to 0.8 V and the charge was limited to 1.65 V for current densities of 35 and 30 mA cm⁻², 1.6 V for 25 and 20 mA cm⁻² and 1.5 V for 10 mA cm⁻² to avoid high voltages and oxygen generation from the water-splitting reaction at the anode. As the current density is increased, the discharge voltage, cycle time and the overall capacity decrease because of the higher overpotential, activation resistance and increased ohmic resistance.[62] At the highest current density, the discharge curve becomes distorted because of zinc plating on the anode, which reduces the amount of electrode active surface available for further reaction (see Fig. S2†). Charge–discharge curves for

batteries comprising KMnO₄-treated NWCF electrodes appear similar to those with untreated NWCF, but are not shown to avoid redundancy.

Polarization curves were developed at flowrates of 10 and 30 mL min⁻¹ to investigate each battery's response to higher current loads and correspondingly higher ion-transfer demands. Before discharging, the battery was charged to 1.5 V at 10 mA cm⁻² (full charge). Fig. 6(b) shows the results of the polarization analysis for the RFB with untreated NWCF electrodes, which includes the discharge voltage *vs.* current density for various electrolyte flow rates, and the power density *vs.* current density. The voltages reported are not IR-corrected because the difference was not significant. As expected, higher discharge voltages, and therefore power density, were achieved with increasing flowrate. In the ZI electrolyte, RFBs with untreated NWCF electrodes had a peak power density of 98 mW cm⁻² (much higher than RFBs with untreated NWCF in vanadium), which is well below that obtained from RFBs with commercial PAN-derived carbon felts (∼145 mW cm⁻²).

Fig. 6(c) shows the polarization curves for RFBs with KMnO₄-treated NWCF and PAN-derived carbon felt electrodes. Compared to RFBs with untreated NWCF electrodes, those with oxidized NWCF showed a 16% improvement in power density, but this is still low relative to the peak power observed in RFBs with PAN-derived carbon felt. While the improvement in battery performance is relatively small, untreated NWCF already performs well in the ZI electrolyte, especially at current



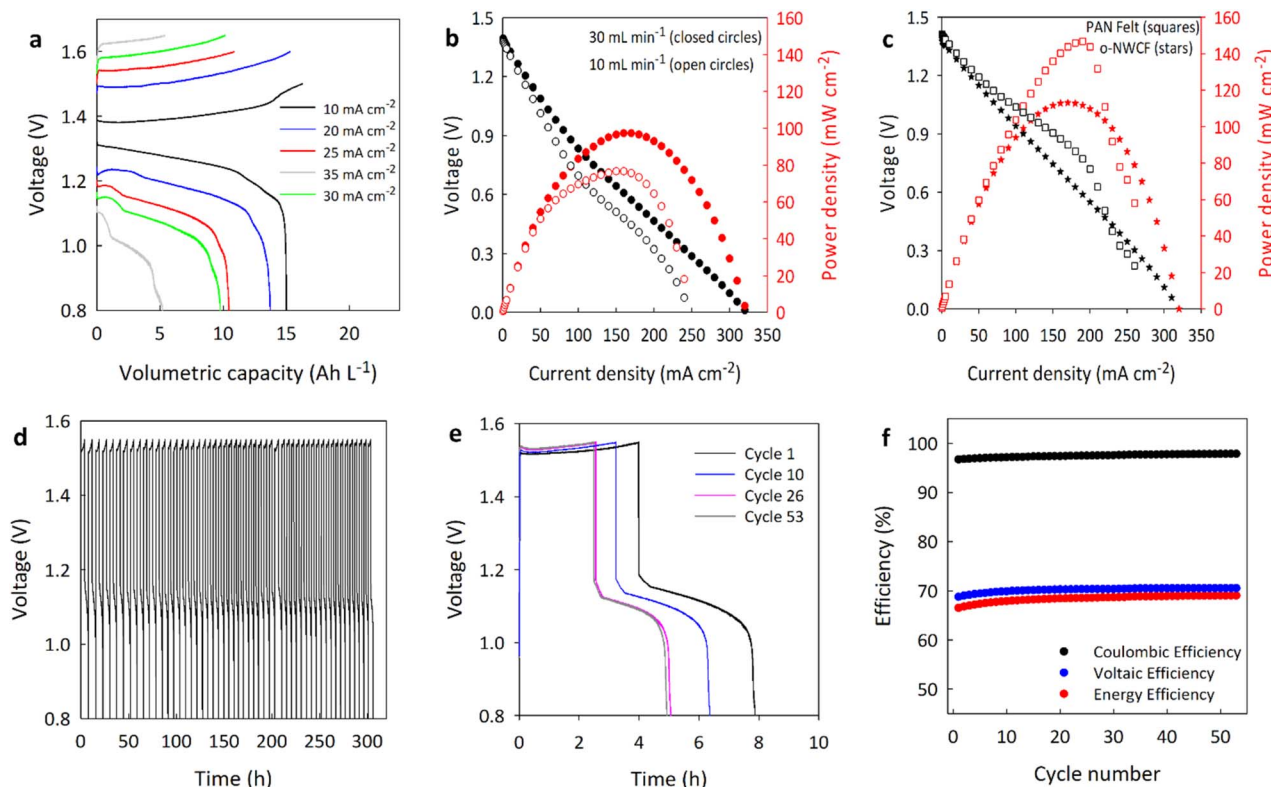**Fig. 6** Electrochemical performance of RFBs with NWCF in zinc iodide. (a) Charge−discharge curves at 30 mL min⁻¹, (b) polarization curves at varying flowrates, (c) polarization curves at 30 mL min⁻¹ for RFBs with KMnO₄-treated NWCF electrodes and PAN-derived carbon felt electrodes, (d−f) cycling performance at 25 mA cm⁻² and 60 mL min⁻¹.

densities up to 100 mA cm$^{-2}$. Although PAN-based felts had higher voltages and power densities there was a significant drop in the voltage profile due to excessive zinc plating and dendrite formation (Fig. S3†).[69] While this is inferior to RFBs with PAN-derived carbon electrodes, we have only been able to perform a single surface treatment, and it's likely the electrode surface requires specific treatment depending on redox electrolyte formulation. One benefit of the untreated NWCF electrodes is the reduction of zinc plating and dendrite formation during battery operation. Selective treatment of electrodes for the anode and cathode could provide a path to improved battery performance, in terms of power and stability, using low-cost pitch-based electrode materials.

The cycling stability was assessed by continuously charging and discharging the RFBs with NWCF electrodes at 25 mA cm$^{-2}$ and a flowrate of 60 mL min$^{-1}$ for over 300 h (53+ cycles), as shown in Fig. 6(d). For clarity, the initial, intermediate and final cycles are shown in Fig. 6(e). Some capacity fading is observed up to about 20 cycles and 130 h due to zinc plating, but it is worth noting that the capacity remains fairly constant for all subsequent cycles. Furthermore, coulombic, voltage, and energy efficiency all remain steady after the initial few cycles, as shown in Fig. 6(f).

## Conclusions

In summary, we've shown that low-cost and sustainable non-woven carbon fiber electrodes, produced from mesophase petroleum-pitch precursor using a scalable melt-blowing process, can perform comparable to benchmark PAN-based electrode materials of redox flow batteries, if not slightly better under typical operating conditions. The development of new electrode materials is often overlooked because the majority of studies to reduce the cost of RFBs are focused on electrolytes and membranes, the two main cost factors in flow batteries. The electrode materials still make up around 12% of the overall flow battery cost and compared to PAN-derived carbon felt electrodes, petroleum pitch-based carbon fiber electrodes can be produced at a fraction of the cost.

Compared to commercial PAN-derived carbon fibers, pitch-based carbon fibers have increased graphitic content, tensile strength, and electrical conductivity. RFBs fabricated with oxidized NWCF electrodes show nearly identical battery performance to those prepared with commercial PAN-derived carbon felts in vanadium electrolytes (peak power density of 137 mW cm$^{-2}$ vs. 139 mW cm$^{-2}$, respectively). Carbon fiber electrodes derived from mesophase pitch even outperform those derived from PAN at current densities below 150 mA cm$^{-2}$. When RFBs with NWCF electrodes are evaluated in a zinc iodide electrolyte, the voltage and power (83 mW cm$^{-2}$) density are slightly lower compared to RFBs with PAN-derived carbon felts (104 mW cm$^{-2}$) @ 100 mA cm$^{-2}$. Because of their low-cost precursor and processing methods, NWCF electrodes offer a promising solution to minimizing the cost and environmental impact of RFB electrode materials. With further optimization of the surface chemistry, which is the primary factor that affects electrochemical behavior of porous and nano/micro-structured carbon materials, these electrodes will likely result in improved battery performance. Thus, highly graphitic electrode materials with optimised performance, produced from low-cost precursors using highly scalable and inexpensive melt-blown method could be an ideal alternative to current commercial carbon felts.

## Data availability

The data supporting this article have been included as ESI.†

## Author contributions

Conceptualization, S. V. K., A. A. W., A. A. O. and M. E. R.; methodology, A. A. W., and S. V. K.; validation, S. V. K. and A. A. W.; investigation, S. V. K. and A. A. W.; writing – original draft S. V. K. and A. A. W.; writing – review and editing S. V. K., A. A. W., A. A. O. and M. E. R.; supervision A. A. O. and M. E. R.

## Conflicts of interest

Authors would like to declare that the intellectual property rights for the research results are being filed.

## Acknowledgements

## References

1 N. A. Sepulveda, J. D. Jenkins, A. Edington, D. S. Mallapragada and R. K. Lester, The design space for long-duration energy storage in decarbonized power systems, Nat. Energy, 2021, 6, 506–516.

2 S. Chu, Y. Cui and N. Liu, The path towards sustainable energy, Nat. Mater., 2017, 16, 16–22.

3 L. Aspitarte and C. R. Woodside, A techno-economic survey of energy storage media for long-duration energy storage applications, Cell Rep. Sustain., 2024, 1, 100007.

4 B. Kroposki, B. Johnson, Y. Zhang, V. Gevorgian, P. Denholm, B.-M. Hodge and B. Hannegan, Achieving a 100% Renewable Grid: Operating Electric Power Systems with Extremely High Levels of Variable Renewable Energy, IEEE Power Energy Mag., 2017, 15, 61–73.

5 J. Salazar, F. Tadeo and C. Prada, Modelling of Diesel Generator Sets That Assist Off-Grid Renewable Energy Micro-grids, Renew. Energy Sustain. Dev., 2015, 1, 72–80.

6 S. Deb, D. Ghosh and D. K. Mohanta, in 2016 International Conference on Electrical, Electronics, and Optimization Techniques (ICEEOT), 2016, pp. 2714–2719.

7 S. Few, O. Schmidt and A. Gambhir, Electrical energy storage for mitigating climate change - Grantham Briefing Paper 20 | Grantham Institute – Climate Change and the Environment, Imperial College London, https://www.imperial.ac.uk/grantham/publications/mitigation/electrical-energy-storage-

for-mitigating-climate-change—grantham-briefing-paper-20.php, accessed 31 January 2024.

8  R. Barbosa, M. Issa, S. Silva and A. Ilinca, Variable Speed Diesel Electric Generators: Technologies, Benefits, Limitations, Impact on Greenhouse Gases Emissions and Fuel Efficiency, *J. Energy Power Technol.*, 2022, **4**, 1–21.

9  P. Albertus, J. S. Manser and S. Litzelman, Long-Duration Electricity Storage Applications, Economics, and Technologies, *Joule*, 2020, **4**, 21–32.

10  H. Chen, T. N. Cong, W. Yang, C. Tan, Y. Li and Y. Ding, Progress in electrical energy storage system: A critical review, *Prog. Nat. Sci.*, 2009, **19**, 291–312.

11  M. Skyllas-Kazacos, M. H. Chakrabarti, S. A. Hajimolana, F. S. Mjalli and M. Saleem, Progress in Flow Battery Research and Development, *J. Electrochem. Soc.*, 2011, **158**, R55.

12  A. Aluko and A. Knight, A Review on Vanadium Redox Flow Battery Storage Systems for Large-Scale Power Systems Application, *IEEE Access*, 2023, **11**, 13773–13793.

13  R. Shan, J. Reagan, S. Castellanos, S. Kurtz and N. Kittner, Evaluating emerging long-duration energy storage technologies, *Renew. Sustain. Energy Rev.*, 2022, **159**, 112240.

14  A. Z. Weber, M. M. Mench, J. P. Meyers, P. N. Ross, J. T. Gostick and Q. Liu, Redox flow batteries: a review, *J. Appl. Electrochem.*, 2011, **41**, 1137.

15  Y. Jiang, Z. Liu, Y. Ren, A. Tang, L. Dai, L. Wang, S. Liu, Y. Liu and Z. He, Maneuverable B-site cation in perovskite tuning anode reaction kinetics in vanadium redox flow batteries, *J. Mater. Sci. Technol.*, 2024, **186**, 199–206.

16  C. Ponce de León, A. Frías-Ferrer, J. González-García, D. A. Szánto and F. C. Walsh, Redox flow cells for energy conversion, *J. Power Sources*, 2006, **160**, 716–732.

17  Z. Yang, J. Zhang, M. C. W. Kintner-Meyer, X. Lu, D. Choi, J. P. Lemmon and J. Liu, Electrochemical Energy Storage for Green Grid, *Chem. Rev.*, 2011, **111**, 3577–3613.

18  C. Choi, S. Kim, R. Kim, Y. Choi, S. Kim, H. Jung, J. H. Yang and H.-T. Kim, A review of vanadium electrolytes for vanadium redox flow batteries, *Renew. Sustain. Energy Rev.*, 2017, **69**, 263–274.

19  K. Jae Kim, M.-S. Park, Y.-J. Kim, J. Ho Kim, S. Xue Dou and M. Skyllas-Kazacos, A technology review of electrodes and reaction mechanisms in vanadium redox flow batteries, *J. Mater. Chem. A*, 2015, **3**, 16913–16933.

20  P. Leung, X. Li, C. Ponce De León, L. Berlouis, C. T. J. Low and F. C. Walsh, Progress in redox flow batteries, remaining challenges and their applications in energy storage, *RSC Adv.*, 2012, **2**, 10125.

21  L. Tang, P. Leung, M. R. Mohamed, Q. Xu, S. Dai, X. Zhu, C. Flox, A. A. Shah and Q. Liao, Capital cost evaluation of conventional and emerging redox flow batteries for grid storage applications, *Electrochim. Acta*, 2023, **437**, 141460.

22  R. M. Darling, K. G. Gallagher, J. A. Kowalski, S. Ha and F. R. Brushett, Pathways to low-cost electrochemical energy storage: a comparison of aqueous and nonaqueous flow batteries, *Energy Environ. Sci.*, 2014, **7**, 3459–3477.

23  P. Spitsen, *Energy Storage Grand Challenge Roadmap*, 2020.

24  Y. Shi, C. Eze, B. Xiong, W. He, H. Zhang, T. M. Lim, A. Ukil and J. Zhao, Recent development of membrane for vanadium redox flow battery applications: A review, *Appl. Energy*, 2019, **238**, 202–224.

25  R. K. Emmett, M. Grady and M. E. Roberts, Increasing Charge Transfer at the Liquid−Solid Interface Using Electrodes Modified with Redox Mediators, *Adv. Energy Sustainability Res.*, 2022, **3**, 2100132.

26  C. Xie, Y. Duan, W. Xu, H. Zhang and X. Li, A Low-Cost Neutral Zinc–Iron Flow Battery with High Energy Density for Stationary Energy Storage, *Angew. Chem., Int. Ed.*, 2017, **56**, 14953–14957.

27  M. C. Tucker, A. Phillips and A. Z. Weber, All-Iron Redox Flow Battery Tailored for Off-Grid Portable Applications, *ChemSusChem*, 2015, **8**, 3996–4004.

28  K. Gong, F. Xu, J. B. Grunewald, X. Ma, Y. Zhao, S. Gu and Y. Yan, All-Soluble All-Iron Aqueous Redox-Flow Battery, *ACS Energy Lett.*, 2016, **1**, 89–93.

29  A. A. Williams, R. K. Emmett and M. E. Roberts, High power zinc iodine redox flow battery with iron-functionalized carbon electrodes, *Phys. Chem. Chem. Phys.*, 2023, **25**, 16222–16226.

30  A. A. Williams, X. Wang, E. M. Davis and M. E. Roberts, Leveraging sulfonated poly(ether ether ketone) for superior performance in zinc iodine redox flow batteries, *J. Energy Storage*, 2023, **73**, 108937.

31  B. Li, Z. Nie, M. Vijayakumar, G. Li, J. Liu, V. Sprenkle and W. Wang, Ambipolar zinc-polyiodide electrolyte for a high-energy density aqueous redox flow battery, *Nat. Commun.*, 2015, **6**, 6303.

32  C. Xie, H. Zhang, W. Xu, W. Wang and X. Li, A Long Cycle Life, Self-Healing Zinc–Iodine Flow Battery with High Power Density, *Angew. Chem., Int. Ed.*, 2018, **57**, 11171–11176.

33  C. M. Fernandez-Marchante, M. Millán, J. I. Medina-Santos and J. Lobato, Environmental and Preliminary Cost Assessments of Redox Flow Batteries for Renewable Energy Storage, *Energy Technol.*, 2020, **8**, 1900914.

34  R. Schweiss, Influence of bulk fibre properties of PAN-based carbon felts on their performance in vanadium redox flow batteries, *J. Power Sources*, 2015, **278**, 308–313.

35  C. Minke, U. Kunz and T. Turek, Carbon felt and carbon fiber - A techno-economic assessment of felt electrodes for redox flow battery applications, *J. Power Sources*, 2017, **342**, 116–124.

36  P. Vass, E. Szabó, A. Domokos, E. Hirsch, D. Galata, B. Farkas, B. Démuth, S. K. Andersen, T. Vigh, G. Verreck, G. Marosi and Z. K. Nagy, Scale-up of electrospinning technology: Applications in the pharmaceutical industry, *Wiley Interdiscip. Rev.: Nanomed. Nanobiotechnology*, 2020, **12**, e1611.

37  P. Morgan, *Carbon Fibers and Their Composites*, CRC Press, 2005.

38  L. Eifert, R. Banerjee, Z. Jusys and R. Zeis, Characterization of Carbon Felt Electrodes for Vanadium Redox Flow Batteries: Impact of Treatment Methods, *J. Electrochem. Soc.*, 2018, **165**, A2577.

39 C. Lai, Z. Zhou, L. Zhang, X. Wang, Q. Zhou, Y. Zhao, Y. Wang, X.-F. Wu, Z. Zhu and H. Fong, Free-standing and mechanically flexible mats consisting of electrospun carbon nanofibers made from a natural product of alkali lignin as binder-free electrodes for high-performance supercapacitors, *J. Power Sources*, 2014, **247**, 134–141.

40 Q. Deng, X.-Y. HuangYang, X. Zhang, Z.-H. Xiao, W.-B. Zhou, H.-R. Wang, H.-Y. Liu, F. Zhang, C.-Z. Li, X.-W. Wu and Y.-G. Guo, Edge-Rich Multidimensional Frame Carbon as High-Performance Electrode Material for Vanadium Redox Flow Batteries, *Adv. Energy Mater.*, 2022, **12**, 2103186.

41 C. Flox, M. Skoumal, J. Rubio-Garcia, T. Andreu and J. R. Morante, Strategies for enhancing electrochemical activity of carbon-based electrodes for all-vanadium redox flow batteries, *Appl. Energy*, 2013, **109**, 344–351.

42 M. G. Huson, in *Structure and Properties of High-Performance Fibers*, Elsevier, 2017, pp. 31–78.

43 J. Sloan, *Composites World Weekly*, 2016.

44 S. Das and P. Nagapurkar, *Sustainable Coal Tar Pitch Carbon Fiber Manufacturing*, 2021.

45 S. V. Kanhere, V. Bermudez and A. A. Ogale, in *Fibre Reinforced composites:Constituents,compatibility,Persepctive and Applications*, ed. J. Kuruvilla, K. Oksman, G. Gejo, R. Wilson and S. Appukuttan, Elsevier, 1st edn, 2021, pp. 273–306.

46 V. Bermudez and A. A. Ogale, Adverse effect of mesophase pitch draw-down ratio on carbon fiber strength, *Carbon*, 2020, **168**, 328–336.

47 K. Christ and K. J. Hüttinger, Carbon-fiber-reinforced carbon composites fabricated with mesophase pitch, *Carbon*, 1993, **31**, 731–750.

48 S. Kanhere, V. Bermudez and A. Ogale, in *SAMPE - Composites and Advanced Materials Expo*, SAMPE, Virtual, 2020.

49 V. Bermudez, S. Lukubira and A. A. Ogale, in *Comprehensive Composite Materials II*, ed. P. W. R. Beaumont and C. H. Zweben, Elsevier, Oxford, 2018, pp. 41–65.

50 N. Takami, A. Satoh, M. Hara and T. Ohsaki, Structural and Kinetic Characterization of Lithium Intercalation into Carbon Anodes for Secondary Lithium Batteries, *J. Electrochem. Soc.*, 1995, **142**, 371.

51 F. Watanabe, Y. Korai, I. Mochida and Y. Nishimura, Structure of melt-blown mesophase pitch-based carbon fiber, *Carbon*, 2000, **38**(5), 741–747.

52 A. D. Vakili and D. F. Rossillon, Process for collection of continuous fibers as a uniform batt, *US Pat.*, US8206640B2, 2012.

53 Z. Yue, C. Liu, A. Vakili, Z. Yue, C. Liu and A. Vakili, Meltblown Solvated Mesophase Pitch-Based Carbon Fibers: Fiber Evolution and Characteristics, *C*, 2017, **3**, 26.

54 M. Baritto, A. O. Oni and A. Kumar, Estimation of life cycle greenhouse gas emissions of asphaltene-based carbon fibers derived from oil sands bitumen, *Sustain. Mater. Technol.*, 2023, **36**, e00627.

55 *ASTM D3379-75: Standard Test Method for Tensile Strength and Young's Modulus for High-Modulus Single-Filament Materials*, 1989, DOI: 10.1520/D3379-75R89E01.

56 B. Shanahan, K. Seteiz, P. A. Heizmann, S. Koch, J. Büttner, S. Ouardi, S. Vierrath, A. Fischer and M. Breitwieser, Rapid wet-chemical oxidative activation of graphite felt electrodes for vanadium redox flow batteries, *RSC Adv.*, 2021, **11**, 32095–32105.

57 R. K. Emmett, M. J. Kowalske, H. Mou, M. Grady, H. Jiang and M. E. Roberts, Creating Faradaic Carbon Nanotube Electrodes with Mild Chemical Oxidation, *Batter. Supercaps*, 2019, **2**, 858–866.

58 G. M. Swain, in *Handbook of Electrochemistry*, ed. C. G. Zoski, Elsevier, Amsterdam, 2007, pp. 111–153.

59 Q. Deng, P. Huang, W.-X. Zhou, Q. Ma, N. Zhou, H. Xie, W. Ling, C.-J. Zhou, Y.-X. Yin, X.-W. Wu, X.-Y. Lu and Y.-G. Guo, A High-Performance Composite Electrode for Vanadium Redox Flow Batteries, *Adv. Energy Mater.*, 2017, **7**, 1700461.

60 C. Xie, Y. Liu, W. Lu, H. Zhang and X. Li, Highly stable zinc–iodine single flow batteries with super high energy density for stationary energy storage, *Energy Environ. Sci.*, 2019, **12**, 1834–1839.

61 D. K. Kim, S. J. Yoon, J. Lee and S. Kim, Parametric study and flow rate optimization of all-vanadium redox flow batteries, *Appl. Energy*, 2018, **228**, 891–901.

62 D. Aaron, Z. Tang, A. B. Papandrew and T. A. Zawodzinski, Polarization curve analysis of all-vanadium redox flow batteries, *J. Appl. Electrochem.*, 2011, **41**, 1175.

63 B. Sun and M. Skyllas-Kazacos, Modification of graphite electrode materials for vanadium redox flow battery application—I. Thermal treatment, *Electrochim. Acta*, 1992, **37**, 1253–1260.

64 C. Zhang, L. Zhang, Y. Ding, S. Peng, X. Guo, Y. Zhao, G. He and G. Yu, Progress and prospects of next-generation redox flow batteries, *Energy Storage Mater.*, 2018, **15**, 324–350.

65 A. Hassan and T. Tzedakis, Facile chemical activation of graphite felt by KMnO4 acidic solution for vanadium redox flow batteries, *Appl. Surf. Sci.*, 2020, **528**, 146808.

66 K. J. Kim, Y.-J. Kim, J.-H. Kim and M.-S. Park, The effects of surface modification on carbon felt electrodes for use in vanadium redox flow batteries, *Mater. Chem. Phys.*, 2011, **131**, 547–553.

67 X. Liu, T. Li, Z. Yuan and X. Li, Low-cost all-iron flow battery with high performance towards long-duration energy storage, *J. Energy Chem.*, 2022, **73**, 445–451.

68 Z. Yuan, Y. Yin, C. Xie, H. Zhang, Y. Yao and X. Li, Advanced Materials for Zinc-Based Flow Battery: Development and Challenge, *Adv. Mater.*, 2019, **31**, 1902025.

69 Q. Chen, S. Chen, J. Ma, S. Ding and J. Zhang, Synergic anchoring of Fe2N nanoclusters on porous carbon to enhance reversible conversion of iodine for high-temperature zinc-iodine battery, *Nano Energy*, 2023, **117**, 108897.